Perturbation theory treatment of pseudorotation in cyclic-N_3

Dmitri Babikov[a)]
Chemistry Department, Marquette University, PO Box 1881, Milwaukee, Wisconsin 53201, USA

(Received 5 December 2010; accepted 16 February 2011; published online 15 March 2011)

A relatively simple treatment using perturbation theory is proposed to describe spectrum of pseudorotational states in cyclic-N_3. The purpose is to develop an analytical expression that could be used to fit the experimentally determined spectrum of cyclic-N_3, with purpose of identifying this molecule in the laboratory and deriving parameters of its potential energy surface directly from the experimental data. The perturbation theory expression derived in this work is used to fit the spectrum calculated numerically in the previous work [D. Babikov and B. Kendrick, J. Chem. Phys. **133**, 174310 (2010)]. It is found that the second order of perturbation theory works well, giving a very good fit of the spectrum, with the rms deviation of only 0.26 cm^{-1}. Analysis reveals that important characteristics of the potential energy surface, such as equilibrium geometry and pseudorotation barriers, are directly related to the features of spectrum, such as splittings, and can be readily derived from experimental data, when those become available. © *2011 American Institute of Physics*. [doi:10.1063/1.3563634]

I. INTRODUCTION

Cyclic-N_3 is a Jahn–Teller molecule that exhibits the seam of conical intersections in the equilateral triangle (D_{3h}) configurations.[1] Due to the Jahn–Teller distortion effect, the minimum energy point on the potential energy surface (PES) of cyclic-N_3 occurs at the isosceles triangle (C_{2v}) configuration and, due to the symmetry, there are three such minima around the conical intersection.[1] Such behavior is quite typical and is found in several other triatomic Jahn–Teller molecules.[2–4] What makes cyclic-N_3 interesting and quite special is the fact that three transition states (between those three minima) occur at very low energies, allowing the motion of nuclei between the three energetically equivalent wells. For comparison, the conical intersection in cyclic-N_3 is at 4599.28 cm^{-1} above the minimum, while energy of the transition state points is only 311.33 cm^{-1}. The vibrational zero-point energy (ZPE) of cyclic-N_3 is 1325.67 cm^{-1}, which is more than enough to go over the transition states easily without any vibrational excitation, by just being in the ground vibrational (highly delocalized) quantum state.[5] The potential energy surface of cyclic-N_3, presented in Fig. 1, reflects these properties and looks like a circular channel surrounding the conical intersection. The depth and shape of this channel changes very little as it encircles the conical intersection. Wave functions of the vibrational states formed in this channel exhibit highly delocalized shapes.[5]

The motion of nuclei along the channel in Fig. 1 represents a mode of vibration, but is called a *pseudorotational motion* because it leads to rotation in space (i) of the principal axes of inertia of the molecule and (ii) of the dipole moment of the molecule, even if the overall rotational state of the molecule is isotropic, $J = 0$.[6] In the case of cyclic-N_3 we can talk about a weakly hindered or an almost free pseudorotation, since the pseudorotational barriers are so low.

The spectrum of vibrational states of cyclic-N_3 was computed in the earlier work.[5] Two sets of results were presented: one based on the standard Born–Oppenheimer (BO) approximation and second based on the generalized Born–Oppenheimer (GBO) treatment, where the geometric phase effect was included in calculations of the vibrational states using gauge theory.[7] This effect originates from the property of electronic wave function to change sign when the motion of nuclei encircles the conical intersection.[8] The total wave function, which is the product of {electronic}×{vibrational}, must remain smooth and continuous in the entire configuration space, which is possible only if the vibrational wave function also changes sign (as vibrational motion encircles the conical intersection).

In cyclic-N_3, where the conical intersection is in the D_{3h} configuration, effect of the geometric phase can be rationalized using a relatively simple picture. The motion that encircles conical intersection is precisely the pseudorotational motion discussed above (see Fig. 1). Thus, geometric phase affects the progression of pseudorotational states only, having essentially no effect on states of the other two modes (bending and breathing). If the geometric phase is neglected, the pseudorotational wave functions are smooth and continuous around the conical intersection and can be described by integer values of the pseudorotational quantum number m.[6] If the geometric phase is included, the pseudorotational wave functions change sign and correspond to *half-integer* values of m. For example, without the geometric phase the ground state of cyclic-N_3 would be an $m = 0$ state of symmetry A_1 at 1310.65 cm^{-1}, described by a nodeless donutlike wave function encircling the conical intersection.[5] When the geometric phase is included, the ground state of cyclic-N_3 is a degenerate $m = 1/2$ state of E-symmetry at 1325.67 cm^{-1}. Its wave function has one node and changes sign as vibrational motion encircles the conical intersection.[5,6] The shift of the ground state by ~15 cm^{-1}, the changes of its symmetry, and degeneracy can be regarded as effects of the geometric phase. For the excited states of cyclic-N_3, such shifts are larger and reach

a)Author to whom correspondence should be addressed. Electronic mail: dmitri.babikov@mu.edu.

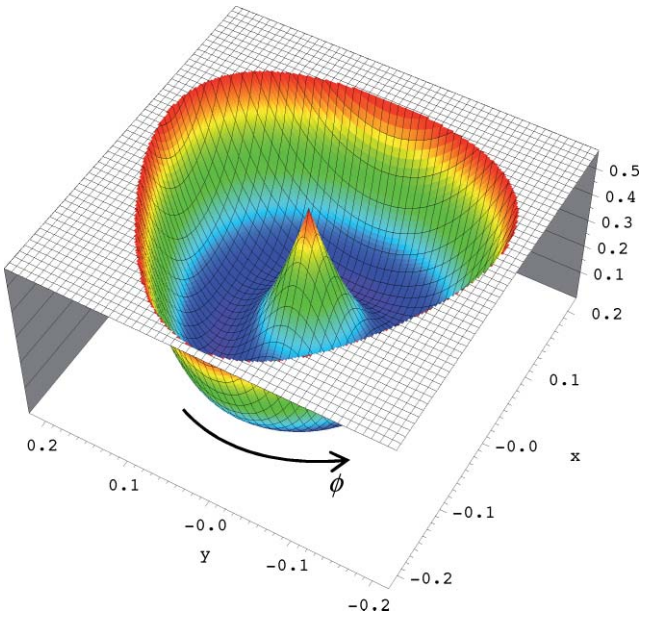

FIG. 1. A two-dimensional slice of the potential energy surface of cyclic-N_3 through the point of conical intersection. Direction of the pseudorotational motion along ϕ is shown by arrow.

a few hundred wave numbers at energies close to the conical intersection.[5] It should be emphasized that in nature only the states with half-integer values of m do exist; the states with integer values of m were computed for methodological purpose only (in order to see differences).

Intensities of the infrared (IR) transitions between the vibrational states of cyclic-N_3 have been computed recently.[6] It was found that the pseudorotational mode is several orders of magnitude brighter compared to the bending and breathing modes. The brightest transitions correspond to $\Delta m = \pm 1$ and, in typical experimental conditions, should involve ten lower energy states, up to $m = 9/2$. Some of these states ($m = 1/2, 5/2, 7/2$) are exactly degenerate pairs of E-symmetry, while others ($m = 3/2, 9/2$) are nondegenerate states of symmetries A_1 and A_2 with nonzero splittings (see Table I). These splittings should manifest in the IR-spectrum of cyclic-N_3 and may help to identify this mysterious molecule in the laboratory.[9–15] It is clear that a rigorous theoretical treatment of the pseudorotational motion, including the geometric phase effect, is essential for the accurate theoretical prediction of the IR-spectrum.

It is also desirable to have better intuitive understanding of the origin of these splittings and develop the means of relating the magnitudes of these splittings to features of the potential energy surface of the molecule. With this purpose in mind we decided to focus on qualitative and quantitative analysis of the lower pseudorotational states of cyclic-N_3 (calculated numerically in the previous work[5,6]) and develop a transparent theoretical treatment for them. In addition to the ten states listed in the previous paragraph, our analysis incorporates some states calculated without inclusion of the geometric phase, namely, $m = 0$, 1, 2, 3, and 4. These states do not occur in nature but they carry accurate information about the potential energy surface, which is important methodologically. For example, a pair of states with $m = 3$ (symmetries A_1 and A_2) show significant splitting, ~ 23 cm^{-1} (see Table I). The states with $m = 1$, 2, and 4 are exactly degenerate.

Figure 1 shows the spectrum of 19 pseudorotational states used in this paper. Some of them, three pairs indicated by arrows in Fig. 1, show splittings in the range between 1 and 100 cm^{-1}. The value of splitting decreases as energy of states increases. In some cases the energy of symmetric state m^+ is below the energy of the antisymmetric state m^- (e.g., $m = 3/2, 9/2$), but there are cases when the order is reversed (e.g., $m = 3$). Six pairs of excited pseudorotational states in Fig. 1 are doubly degenerate. At lower energies the spectrum in Fig. 1 is near parabolic, typical to a rotor, but at higher energies (especially those outside of the range shown in Fig. 1) the spectrum flattens out toward a linear, typical to harmonic oscillator. Can we explain all these features in a simple intuitive manner? Can we reproduce them accurately using a simple model spectroscopy-kind Hamiltonian?

The paper is organized as follows. In Sec. II we describe the Hamiltonian and develop the theoretical framework (perturbation theory) used to derive analytical expression for the pseudorotational spectrum of cyclic-N_3. In Sec. III this expression is used to fit the spectrum of pseudorotational states calculated numerically in the previous work. Conclusions are given in Sec. IV.

II. PERTURBATION THEORY TREATMENT OF PSEUDOROTATION

Using the adiabatically-adjusting principal-axes hyperspherical (APH) coordinates[16] the Hamiltonian operator for nuclear motion of a nonrotating triatomic molecule ($J = 0$) is expressed as[17]

$$H_{J=0} = -\frac{1}{2\mu\rho^5}\frac{\partial}{\partial\rho}\rho^5\frac{\partial}{\partial\rho} - \frac{2}{\mu\rho^2}\frac{1}{\sin 2\theta}\frac{\partial}{\partial\theta}\sin 2\theta\frac{\partial}{\partial\theta} + \frac{2}{\mu\rho^2\sin^2\theta}\left(-i\frac{\partial}{\partial\phi}\right)^2 + V(\rho,\theta,\phi), \quad (1)$$

where $\mu = \sqrt{m_1 m_2 m_3/(m_1+m_2+m_3)}$ is a three body reduced mass. Numerical calculations of vibrational eigenstates in cyclic-N_3 for energies up to the conical intersection (~ 4600 cm^{-1}) using this exact Hamiltonian were reported in our earlier work.[5,6] Here we develop a simplified analytic approach to characterize and better understand the lower part of this spectrum, important for the IR-spectroscopy. We assume that the vibrational excitation is low, and the three vibrational modes are coupled weakly. Our earlier numerical results[5,6] support this assumption. Among the three APH coordinates, the hyper-radial coordinate ρ describes the symmetric stretching motion, or the breathing mode, while the hyperangle θ describes the bending mode. In the majority of molecules the motion along the hyperangle ϕ is restricted, by the potential energy surface $V(\rho,\theta,\phi)$, to the vicinity of the equilibrium position and corresponds to the asymmetric stretching mode [one example is a molecule of ozone, O_3 (Ref. 18)]. However, in the cyclic-N_3 the large amplitude motion along the hyperangle ϕ is allowed (by zero-point energy), which leads to the transformation of the asymmetric stretching mode into the pseudorotational motion around the

TABLE I. The spectrum (in cm^{-1}) of pseudorotational states in cyclic-N_3 computed numerically (from Ref. 5) and its fit using analytical expressions of various orders of the perturbation theory. δE is the residual deviation of the exact result from the fit.

	Numerical	Zeroth order		First order		Second order		Third order	
m and symmetry	E	E	δE	E	δE	E	δE	E	δE
0	1310.65	1306.05	4.60	1306.05	4.60	1310.72	−0.07	1310.32	0.33
$1/2^{\pm}$	1325.67	1324.66	1.01	1324.66	1.01	1325.54	0.13	1325.47	0.20
$1^{\pm}$	1364.95	1375.47	−10.52	1375.47	−10.52	1365.15	−0.20	1362.51	2.44
$3/2^{+}$	1401.22	1452.45	−51.23	1402.22	−1.00	1400.99	0.23	1405.88	−4.66
$3/2^{-}$	1501.68	1452.45	49.23	1502.68	−1.00	1501.45	0.23	1503.38	−1.70
$2^{\pm}$	1560.68	1551.07	9.61	1551.07	9.61	1561.12	−0.44	1556.16	4.52
$5/2^{\pm}$	1668.88	1667.87	1.01	1667.87	1.01	1669.00	−0.12	1669.46	−0.58
3^{-}	1787.52	1800.14	−12.62	1788.86	−1.34	1787.43	0.09	1788.02	−0.50
3^{+}	1810.07	1800.14	9.93	1811.41	−1.34	1809.98	0.09	1810.58	−0.51
$7/2^{\pm}$	1944.56	1945.74	−1.18	1945.74	−1.18	1944.14	0.42	1944.07	0.49
$4^{\pm}$	2101.70	2102.97	−1.27	2102.97	−1.27	2102.25	−0.55	2101.71	−0.01
$9/2^{+}$	2269.93	2270.44	−0.51	2269.22	0.71	2269.84	0.09	2269.94	−0.01
$9/2^{-}$	2272.38	2270.44	1.94	2271.67	0.71	2272.29	0.09	2272.39	−0.01

conical intersection,[1] described by $-\pi < \phi < +\pi$. As the pseudorotational motion encircles the conical intersection the other two coordinates, ρ and θ, change very little and remain approximately equal to their equilibrium values, ρ_{eq} and θ_{eq} (see Fig. 1). Thus, the pseudorotational mode can be approximately separated from the other two modes and the Hamiltonian of Eq. (1) can be transformed into the following one-dimensional operator:

$$H_{1D} = \mathrm{ZPE} - \frac{1}{2I_m}\frac{\partial^2}{\partial\phi^2} + V(\rho_{eq}, \theta_{eq}, \phi), \tag{2}$$

where ZPE represents the zero-point energy of the breathing and bending modes due to the first two terms in the fully dimensional expression of Eq. (1). Here we focus on the pseudorotational excitation with no breathing and/or bending excitation, so the ZPE is just a constant number. It can be easily estimated from the numerical results of Ref. 5. Using the harmonic oscillator model for the first excited breathing and bending states of cyclic-N_3, we obtain ZPE = 1182.3 cm^{-1}. Using a more sophisticated six-parameter Dunham expansion for these two modes gives the value just slightly higher: ZPE = 1202.1 cm^{-1}.

Note that in Eq. (2) we introduced the *pseudorotational moment of inertia* as

$$I_m = \frac{\mu\rho_{eq}^2 \sin^2\theta_{eq}}{4}. \tag{3}$$

At the basic level the value of I_m can be estimated using parameters of the minimum on the potential energy surface. Using the values of $\rho_{eq} = 3.4656$ bohr and $\tan(\theta_{eq}/2) = 0.1079$ from Ref. 5 and the reduced mass of cyclic-N_3, $\mu = 8.083$amu, we obtain the value of $I_m = 9.172 \times 10^{-3}$ cm.

A. Zero-order model

At the zeroth order of theory we simply neglect the pseudorotational barriers on the PES, which makes the PES flat for the motion encircling the conical intersection, i.e., constant and equal to zero. This is justified by the fact that energies of these barriers, 311.3 cm^{-1}, are small compared to the zero-point energy of the vibrational motion.[6] Barriers to pseudorotation will be treated as a perturbation at the next level of theory.

With the kinetic energy $V = 0$, the zeroth-order (unperturbed) Hamiltonian is

$$H^{(0)} = \mathrm{ZPE} - \frac{1}{2I_m}\frac{\partial^2}{\partial\phi^2} = \mathrm{ZPE} + \frac{\hat{J}_m^2}{2I_m}, \tag{4}$$

where we introduced operator of the pseudorotational angular momentum as $\hat{J}_m = -i\partial/\partial\phi$. Hamiltonian of Eq. (4) describes a one-dimensional rotor or a pseudorotor to be exact. Note that except for the constant ZPE shift, this Hamiltonian corresponds to a textbook example of "particle-on-a-ring" problem with known analytic solutions to energies

$$E_m^{(0)} = \mathrm{ZPE} + \frac{m^2}{2I_m}, \tag{5}$$

and wave functions

$$|m^+\rangle = \frac{1}{\sqrt{\pi}}\cos(m\phi), \tag{6a}$$

$$|m^-\rangle = \frac{i}{\sqrt{\pi}}\sin(m\phi), \tag{6b}$$

where the pseudorotational quantum number m is introduced. Note that normalization condition for the $m = 0$ function requires that $|0\rangle = 1/\sqrt{2\pi}$. Except the $m = 0$ case, the zeroth-order solutions are exactly doubly degenerate, with one wave function in each pair being symmetric and one being antisymmetric. The $m = 0$ function is, obviously, symmetric.

The spectrum of Eq. (5) contains two parameters and, in principle, one can attempt to fit the spectrum of Fig. 2 with Eq. (5). The results are presented in Sec. III and, as one might expect, the quantitative agreement is quite poor although the overall near-parabolic dependence is qualitatively reproduced. We found that a significant improvement is obtained if instead of a single parameter I_m the three parameter

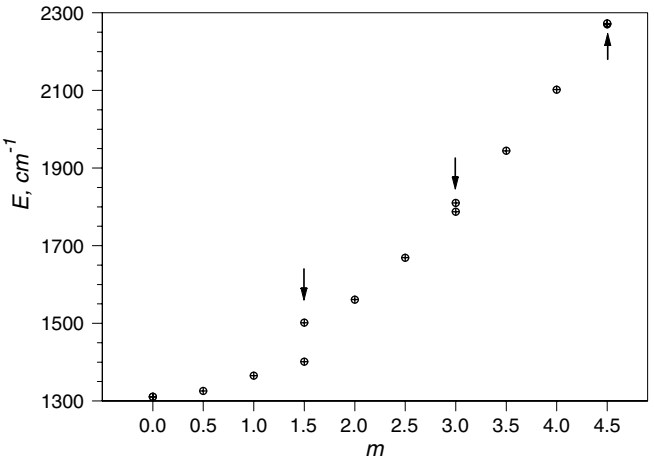

FIG. 2. Lower part of the pseudorotational progression of states of cyclic-N_3. Both BO and GBO states are included (integer and half-integer values of *m,* respectively). Arrows indicate the *A*-symmetry states where the splittings are observed. Circles indicate energies computed numerically in Ref. 5; pluses indicate analytical fit to numerical data using the perturbation theory of second order.

expansion,

$$I_m = I_0 + I_1 m + I_2 m^2, \tag{7}$$

is substituted into Eq. (5). Such expansion takes into account the fact that moment of inertia of the pseudorotor can slightly increase as the pseudorotational excitation increases. This effect is similar to the familiar centrifugal distortion, but may also include the effect of distortion of the PES shape, which is not a perfect ring at higher excitation energies. For the overall approach to be correct and the description of the spectrum to be accurate, we should require $I_0 \gg I_1 \gg I_2$ as a convergence criterion.

Another obvious deficiency of Eq. (5) is the absence of splittings of the states of *A*-symmetry. One can say that the zeroth-order theory does not differentiate between the *A*- and *E*-symmetry states, simply because the zero-order potential $V = 0$ has no threefold symmetry (of the actual PES) built in.

B. First-order correction

The perturbation to the zeroth-order potential is described as a sum of terms

$$V(\phi) = \sum_n V^{[n]}(\phi) = \sum_n V_n \frac{1 - \cos n\phi}{2}, \tag{8}$$

where $\{V_n\}$ is a set of suitable numbers. Since the potential energy surface is threefold symmetric, only the terms with $n = 3$, 6, 9, etc., are allowed in Eq. (8). The first term with $n = 3$ creates three equivalent minima on the PES separated by three pseudorotation barriers, making the pseudorotation hindered at the first order of theory. Necessity of the terms with $n = 6$ and $n = 9$ will be discussed below. Again, for convergence one should require $|V_3| \gg |V_6| \gg |V_9|$, etc.

The matrix elements of the perturbation operator in the basis of zeroth-order wave functions, $H^{(0)}_{mm'}$, are separately computed analytically for each term in the sum of Eq. (8) and can be summarized in the following form:

$$\langle m^+|V^{[n]}|m'^+\rangle = V_n/2, \quad \text{if} \quad m = m', \tag{9a}$$

$$= -V_n/4, \quad \text{if} \quad m = m' \pm n, \tag{9b}$$

$$= -V_n/4, \quad \text{if} \quad m + m' = n. \tag{9c}$$

$$\langle m^-|V^{[n]}|m'^-\rangle = V_n/2, \quad \text{if} \quad m = m', \tag{10a}$$

$$= -V_n/4, \quad \text{if} \quad m = m' \pm n, \tag{10b}$$

$$= +V_n/4, \quad \text{if} \quad m + m' = n. \tag{10c}$$

The special important case is

$$\langle 0|V^{[n]}|m^+\rangle = \frac{-\sqrt{2}V_n}{4}, \text{if } m = n. \tag{11}$$

All other combinations of the indexes m, m', and n lead to zero matrix elements due to cancellation of the integrand. All matrix elements between the symmetric and antisymmetric functions $\langle m^-|V^{[n]}|m'^+\rangle$ vanish due to symmetry. These matrix elements are computed using standard table integrals of trigonometric functions and trigonometric relations. In the literature they have been computed and used before.[19]

The first-order correction to energies requires the diagonal matrix elements only, $m = m'$. Thus, for majority of symmetric and antisymmetric states (exceptions are discussed further) only the expressions of Eq. (9a) or (10a), respectively, should be applied, leading to the constant shift by $V_n/2$ for all values of m and n (all states and all terms of perturbation).

However, for every given n there exists one value of $m = n/2$ (integer or half-integer) such that the condition $m + m' = n$ is also satisfied, simultaneously with $m = m'$ condition. Consequently, the contribution from Eqs. (9c) and (10c) should also be included. One of those comes with a negative sign, $\langle m^+|V^{[n]}|m^+\rangle = -V_n/4$ in Eq. (9c), while the other comes with a positive sign, $\langle m^-|V^{[n]}|m^-\rangle = +V_n/4$ in Eq. (10c), leading to the *splitting* by the value of $V_n/2$ of the symmetric and antisymmetric states with $m = n/2$. For example, the $m = 3/2$ states will split due to V_3, the $m = 3$ states will split due to V_6, and the $m = 9/2$ states will split due to V_9, etc. So, at the first order of theory the states of *A*-symmetry split, while the states of *E*-symmetry remain exactly degenerate. It is important that the median value of the shift for each pair of the split states equals to $V_n/2$, same as the shift for the degenerate states.

In a concise form these results can be written as follows:

$$E^{(1)}_m = H^{(0)}_{mm} = \sum_n \frac{V_n}{2}\left[1 - \delta_{m,n/2}\frac{1}{2}s\right]. \tag{12}$$

Here, $s = 1$ for the $|m^+\rangle$ states, while $s = -1$ for the $|m^-\rangle$ states; the standard Cronicker delta-symbol is used. One can interpret this result in the following way: The first-order correction shifts the entire spectrum (every m) by the same value of $\sum_n V_n/2$, but also splits the pairs of degenerate states, each individually by the value of $V_{2m}/2$. Since only V_3, V_6, V_9, etc.,

are present in the expansion of Eq. (8), the splitting occurs only for $m = 3/2, 3, 9/2$, etc., states.

Analysis of the spectrum presented in Table I shows that the first order of perturbation theory is qualitatively consistent with the numerical results. The values of splittings are $\Delta_{3/2} = 100.46\ \text{cm}^{-1}$, $\Delta_3 = -22.55$, and $\Delta_{9/2} = 2.45\ \text{cm}^{-1}$ (for the states $m = 3/2$, 3, and 9/2, respectively), which gives us information about the magnitudes of parameters V_n in the cyclic-N_3. Using $V_{2m} = 2\Delta_m$ we obtain quick estimates for $V_3 = 200.92\ \text{cm}^{-1}$, $V_6 = -45.10\ \text{cm}^{-1}$, and $V_9 = 4.90\ \text{cm}^{-1}$. Note that the value of V_6 is negative, simply because the $|3^-\rangle$ state lies below the $|3^+\rangle$ state. We also see that the condition $|V_3| \gg |V_6| \gg |V_9|$ is well satisfied.

C. Second-order correction

At the second order of theory the nonzero off-diagonal elements of $H^{(0)}_{mm'}$ will contribute to the correction and we have to identify all such nonzero interactions for every state. The derivations are not very complicated but are somewhat tedious. We will only summarize our procedure using Fig. 3. The main idea here is that due to a given term $V^{[n]}$ in the perturbation potential of Eq. (8) every state $|m\rangle$ interacts with at most two states: $|m'\rangle = |m \pm n\rangle$. This is shown schematically in Fig. 3 by the bows connecting each state to the other states; majority of states $|m\rangle$ are connected to two $|m'\rangle$ states: the $|m-n\rangle$ and $|m+n\rangle$ states. Contributions of different $V^{(n)}$ terms are shown separately in Fig. 3; the integer and half-integer values of m are also separated for clarity. Thus, the matrix elements of Eqs. (9b) and (10b) should be included, which leads to a "general pattern" of the second-order correction in the form of

$$\begin{aligned} E^{(2)}_{m\neq n/2} &= \sum_{m'\neq m} \frac{|H^{(0)}_{mm'}|}{E^{(0)}_m - E^{(0)}_{m'}} \\ &= \frac{|H^{(0)}_{m,m-n}|}{E^{(0)}_m - E^{(0)}_{m-n}} + \frac{|H^{(0)}_{m,m+n}|}{E^{(0)}_m - E^{(0)}_{m+n}} \\ &= \sum_n \left(\frac{V_n}{4}\right)^2 \frac{I_m}{m^2 - (n/2)^2}. \end{aligned} \tag{13}$$

One can see, however, that the expression of Eq. (13) is singular when $m = n/2$. Such cases correspond to $m < n$, when the $|m-n\rangle$ state does not exists and only one matrix element, corresponding to the $|m+n\rangle$ state, can be included. This leads to a special expression for the $m = n/2$ cases

$$E^{(2)}_{m=n/2} = \frac{|H^{(0)}_{m,m+n}|}{E^{(0)}_m - E^{(0)}_{m+n}} = \sum_n \left(\frac{V_n}{4}\right)^2 \frac{I_m}{-n^2}. \tag{14}$$

Several such cases are indicated in Fig. 3 by empty circles.

Furthermore, the case $m = n$ is also special, because $m' = m - n = 0$ and $|m'\rangle = |0\rangle$. The point here is that one state of the pair, the symmetric state $|m^+\rangle$, will interact with $|0\rangle$ state according to Eq. (11), while the other, the antisymmetric state $|m^-\rangle$, will not due to symmetry. As a result, the $|m^+\rangle$ state will be shifted up by $2(V_n/4)^2 2I_m/m^2$compared

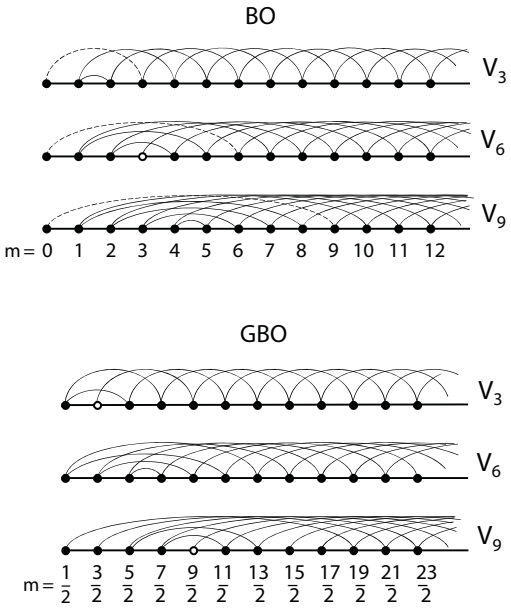

FIG. 3. Schematic representation of interactions between pseudorotational states (labeled by m) due different terms V_n in the perturbation potential of Eq. (8). The integer (BO) and half-integer (GBO) cases are shown separately. Dots represent states, while bows represent interactions. The main "pattern" of interaction is $m' = m \pm n$ (solid bows) and majority of states interact with two other states. Empty circles indicate rare states that interact with only one other state. Dashed bows indicate interactions with the $m' = 0$ state responsible for splittings (at the first order of theory) of the symmetric and antisymmetric states of the A-symmetry.

to the corresponding $|m^-\rangle$ state, which will result in appearance of another kind of splittings at the second order of theory. (Note that both states do interact with the upper state $m' = m + n$ to the equal extend.) Since we have only integer values on n, this splitting will affect only the states with integer m, for example, at the second order the $|3^+\rangle$ and $|3^-\rangle$ states will gain extra splitting due to V_3, etc. It is possible to show that the median value of energy for a pair of such split states will conform to the same general pattern of Eq. (13). Several such cases are indicated in Fig. 3 by dashed bows connecting $m = n$ states to the $m' = 0$ state.

Finally, for a given n, several states with $m < n$ interact with the states $m' = n - m$, $m' \neq m$, according to Eqs. (9c) and (10c). Such interactions create irregularities in the pattern of bows in Fig. 3, mostly in the regions of small values of m. For example, the V_3 creates interaction between $m = 1$ and $m' = 2$, but also between $m = 1/2$ and $m' = 5/2$. Although such cases are treated separately, the final result appears to conform to the general expression given by Eq. (13).

All together these effects can be combined in the following final expression:

$$\begin{aligned} E^{(2)}_m = &\sum_n \left(\frac{V_n}{2}\right)^2 \frac{I_m}{4n^2} \\ &\times \left(\delta_{m,n} 2s + \begin{cases} \frac{1}{(m/n)^2 - (1/2)^2}, & \text{if} \quad m \neq n/2 \\ -1, & \text{if} \quad m = n/2 \end{cases}\right). \end{aligned} \tag{15}$$

We see that the second-order correction plays a very important role because it introduces the m-dependent shifts of

individual states, while the first-order correction gives only the m-independent shift of the entire zeroth-order spectrum by a constant number. Note that the second-order correction affects the splittings of states with integer values of m only, i.e., affects only the splittings of the BO states.

D. Third-order correction

The third order of theory uses ideas of the first and second orders. For the purpose of brevity we skip the derivations and give the final result

$$E_m^{(3)} = -H_{mm}^{(0)} \sum_{m' \neq m} \frac{|H_{mm'}^{(0)}|^2}{\left(E_m^{(0)} - E_{m'}^{(0)}\right)^2}$$

$$= -\sum_n \left(\frac{V_n}{2}\right)^3 \frac{I_m^2}{2n^4} \left(\delta_{m,n} 2s + \left[1 - \delta_{m,n/2} \frac{1}{2} s\right] \right.$$

$$\left. \times \begin{cases} \dfrac{(m/n)^2 + (1/2)^2}{[(m/n)^2 - (1/2)^2]^2}, & \text{if} \quad m \neq n/2 \\ 1/2, & \text{if} \quad m = n/2 \end{cases} \right). \tag{16}$$

This correction includes additional m-dependent shifts of all states as well as splittings of all A-symmetry states with both integer and half-integer values of m.

III. DATA FIT AND ANALYSIS OF RESULTS

At the third order of theory we obtain the following expression for the spectrum:

$$E_m = E_m^{(0)} + E_m^{(1)} + E_m^{(2)} + E_m^{(3)}. \tag{17}$$

This expression uses Eqs. (5), (12), and (14)–(16) and assumes the expansions of Eqs. (7) and (8). In this section we try to fit the numerical spectrum of Table I with the analytical expression (17) by varying the values of parameters. If we want to reproduce splittings of the states up to $m = 9/2$ we must include the terms up to $V^{[9]}$ in the expansion of Eq. (8). This gives us seven fitting parameters: ZPE, I_0, I_1, I_2, V_3, V_6, and V_9. The data in Table I contain 13 points to fit. Due to the complexity of Eqs. (14)–(16) we could not use any standard software package to carry out the fit. We wrote our own nonlinear fitting code that employs iterative procedure of the Levenberg–Marquardt method described in the Numerical Recipes.[20] The derivatives $\partial E_m/\partial(ZPE)$, $\partial E_m/\partial I_0$, $\partial E_m/\partial I_1$, $\partial E_m/\partial I_2$, $\partial E_m/\partial V_3$, $\partial E_m/\partial V_6$, and $\partial E_m/\partial V_9$ needed for this method were obtained by analytical differentiation of Eq. (17) with Eqs. (5), (12), and (14)–(16) and Eqs. (7) and (8). For the purpose of brevity we do not present these expressions here, but our FORTRAN code is available for download to all interested readers.[21] For the initial values of fitting parameters we used the estimated values of ZPE, I_0, V_3, V_6, and V_9 given in Sec. II. For the initially unknown values of I_1 and I_2 we set $I_1 = I_0/10$ and $I_2 = I_0/100$. We also checked and found that the final results are insensitive to the initial values chosen. In all the cases less than 30 iterations were enough to obtain the converged results. All data points were given equal weights in the fitting procedure.

Table I summarizes results of our fitting using various orders of theory, from zeroth order (four-parameters fit, since all $V_n = 0$) to the third order. Our first conclusion is that the results of all orders of theory are consistent and qualitatively similar. They all follow the trend of numerical data. The zeroth-order fit shows no splittings as expected, while the first order reproduces the values of all three splittings perfectly well. The best fit is obtained by the second-order expression. The fact that the third order of perturbation theory gives result inferior to the second order is well known. We did not attempt the fourth order of theory simply because the second-order result is good enough. The maximum deviation of the second-order fit from the numerical results is found for the state $m = 4$ and is only 0.55 cm^{-1}. The rms deviation of the second-order fit is only 0.26 cm^{-1}.

Table II summarizes the final (converged) fitting parameters for various orders of theory. The values of converged fitting parameters ZPE, I_0, V_3, V_6, and V_9 are, in fact, close to the values obtained from simple estimates in Section II. We also see that the $I_0 \gg I_1 \gg I_2$ condition is fulfilled for all orders of theory. The overall contribution of the I_2 term is very small, so that there is no reason to include the higher order terms. Note that the values of I_0, I_1, and I_2 remain unchanged when we go from the zeroth-order theory to the first-order theory. This reflects the fact that the first-order correction shifts the entire spectrum as a whole (and splits the A-symmetry states) without changing the overall shape of the spectrum. The second-order correction significantly affects the value of V_6 (because it changes the splitting of the $m = 3$ state), leaving

TABLE II. The values of fitting parameters for analytical representation of the pseudorotational spectrum of cyclic-N_3 at various orders of the perturbation theory.

	Zeroth order	First order	Second order	Third order
ZPE, cm^{-1}	1306.05	1225.70	1228.06	1233.13
V_3, cm^{-1}	0.00	200.92	200.92	195.37
V_6, cm^{-1}	0.00	−45.10	−23.91	−29.23
V_9, cm^{-1}	0.00	4.90	4.90	4.90
I_0, cm	6.230×10^{-3}	6.230×10^{-3}	7.377×10^{-3}	6.815×10^{-3}
I_1, cm	9.807×10^{-4}	9.807×10^{-4}	6.178×10^{-4}	8.895×10^{-4}
I_2, cm	-7.102×10^{-6}	-7.101×10^{-6}	2.444×10^{-5}	-8.690×10^{-6}
χ^2, cm^{-2}	5539.03	235.67	0.88	52.23

the values of V_3 and V_9 unchanged and equal to those of the first-order theory. Then, the values of V_3 and V_6 change when we go from the second to the third order, while the value of V_9 remains the same. It appears that the value of V_9 is insensitive to the third-order correction simply because the effect of the third order (and probably of all higher orders) is negligible for this excited state. This feature is consistent with the general property of the perturbation theory—effect of the perturbation is higher for the lower energy states and becomes negligible at high energies. Thus we conclude that the value of V_9 is completely defined by the first-order theory, i.e., directly by the splitting of the $m = 9/2$ states: $\Delta_{9/2} = 2.45\ \text{cm}^{-1}$ and $V_9 = 2\Delta_{9/2} = 4.90\ \text{cm}^{-1}$.

Table II also gives the values of the χ^2 deviation that characterizes quality of the nonlinear fit.[20] Here we see again that the second order of theory gives the best description. The third order, although is worse than the second order, is much better than the first order, which is attributed, of course, to the m-dependent shifts of states in the theories beyond the first order. The quantitative success of the second-order expression demonstrated here suggests that this formula can be confidently used for the analysis of the experimental data. Results of the second-order fit are plotted in Fig. 2 (pluses) together with numerical data (circles) and are basically indistinguishable from them at the scale of Fig. 1.

IV. CONCLUSIONS

In this work, using relatively simple tools of the perturbation theory, we were able to reproduce the pseudorotational spectrum of the cyclic-N_3 obtained in the previous work using very sophisticated numerical methodology.[5] All features of the spectrum are reproduced quantitatively and become qualitatively transparent. Thus, the states of E-symmetry are exactly degenerate, while states of A-symmetry split (except the ground state $m = 0$). This is due to the fact that the PES is threefold symmetric, which creates perturbation only in the states with $m = 3/2, 6/2, 9/2$, etc. The value of splitting decreases as energy of state increases, which is a general property of the perturbation effect. Order of the nondegenerate $m = 3$ states is reversed, which is attributed to the negative sign of the V_6 term in the perturbation. At low energies the spectrum is near parabolic, as a spectrum of a rotor. Increase of the pseudorotational excitation leads to distortion of the molecular shape and increase of the pseudorotational moment of inertia, which leads to flattening of the spectrum at high energies.

Obtaining the values of ZPE, I_0, I_1, and I_2 parameters requires numerical nonlinear fitting of the data, while other parameters can be obtained immediately from the values of splittings. For example, the value of V_3 is simply a factor of 2 greater than the splitting of $m = 3/2$ states. The value of V_9 is simply a factor of 2 greater than the splitting of states $m = 9/2$. The sign of V_6 is predicted to be negative; its accurate determination requires second order of perturbation theory.

Overall, the fit of accurate numerical data by the model Hamiltonian is excellent, which gives us reason to believe that it should also be possible to fit experimental data, when those become available, in order to derive parameters of the pseudorotational Hamiltonian (ZPE, I_0, I_1, I_2, V_3, V_6, and V_9) from the experiment and identify cyclic-N_3 in the laboratory.

ACKNOWLEDGMENTS

This work was supported by the Air Force Office of Scientific Research under Grant No. FA9550-09-1-0604. Scott Reid at Marquette University is acknowledged for many fruitful discussions. This research used resources of the National Energy Research Scientific Computing Center, which is supported by the Office of Science of the U.S. Department of Energy under Contract No. DE-AC02-05CH11231.

[1] D. Babikov, P. Zhang, and K. Morokuma, J. Chem. Phys. **121**, 6743 (2004).
[2] T. C. Thompson, D. G. Truhlar, and C. A. Mead, J. Chem. Phys. **82**, 2392 (1985).
[3] M. Keil, H.-G. Krämer, A. Kudell, M. A. Baig, J. Zhu, W. Demtröder, and W. Meyer, J. Chem. Phys. **113**, 7414 (2000).
[4] B. K. Kendrick, Phys. Rev. Lett. **79**, 2431 (1997).
[5] D. Babikov, B. Kendrick, P. Zhang, and K. Morokuma, J. Chem. Phys. **122**, 44315 (2005).
[6] D. Babikov and B. Kendrick, J. Chem. Phys. **133**, 174310 (2010).
[7] B. K. Kendrick and R. T. Pack, J. Chem. Phys. **106**, 3519 (1997).
[8] B. K. Kendrick, Int. J. Quantum. Chem. **64**, 581 (1997).
[9] V. A. Mozhayskiy, D. Babikov, and A. I. Krylov, J. Chem. Phys. **124**, 224309 (2006).
[10] D. Babikov, V. A. Mozhayskiy, and A. I. Krylov, J. Chem. Phys. **125**, 84306 (2006).
[11] N. Hansen, A. M. Wodtke, S. J. Goncher, J. Robinson, N. Sveum, and D. M. Neumark, J. Chem. Phys. **123**, 104305 (2005).
[12] P. Samartzis, J. J.-M. Lee, T.-T. Ching, C. Chadhuri, Y. T. Lee, and A. M. Wodtke, J. Chem. Phys. **123**, 051101 (2005).
[13] P. Samartzis, J. J.-M. Lee, T.-T. Ching, C. Chadhuri, Y. T. Lee, and A. M. Wodtke, J. Chem. Phys. **126**, 041101 (2007).
[14] P. Samartzis and A. M. Wodtke, Int. Rev. Phys. Chem. **25**, 527 (2006).
[15] P. Samartzis and A. M. Wodtke, Phys. Chem. Chem. Phys. **9**, 3054 (2007).
[16] R. T. Pack and G. A. Parker, J. Chem. Phys. **87**, 3888 (1987).
[17] B. K. Kendrick, R. T. Pack, R. B. Walker, and E. F. Hayes, J. Chem. Phys. **110**, 6673 (1999); and references therein.
[18] D. Babikov, B. Kendrick, R. B. Walker, R. T. Pack, P. Fleurat-Lesard, and R. Schinke, J. Chem. Phys. **118**, 6298 (2003).
[19] A. S. Huber, R. D. Gordon, S. A. Reid, and J. D. McDonald, J. Chem. Phys. **97**, 2338 (1992).
[20] W. H. Press, S. A. Teukolsky, W. T. Vetterling, and B. P. Flannery, *Numerical Recipes*, 3rd ed. (Cambridge University Press, 2007).
[21] See supplementary material at http://dx.doi.org/10.1063/1.3563634 for description and source files of our fitting code.